

# Conformational Dynamics Guides Coherent Exciton Migration in Conjugated Polymer Materials: A First-Principles Quantum Dynamical Study

Robert Binder,<sup>†</sup> David Lauvergnat,<sup>‡</sup> and Irene Burghardt<sup>†\*</sup>

<sup>†</sup>*Institute of Physical and Theoretical Chemistry, Goethe University Frankfurt, Max-von-Laue-Str. 7, 60438 Frankfurt, Germany*

<sup>‡</sup>*Laboratoire de Chimie Physique, Université Paris-Sud, UMR 8000, 91405 Orsay, France*

(Dated: November 21, 2017)

We report on high-dimensional quantum dynamical simulations of torsion-induced exciton migration in a single-chain oligothiophene segment comprising twenty repeat units, using a first-principles parametrized Frenkel  $J$ -aggregate Hamiltonian. Starting from an initial inter-ring torsional defect, these simulations provide evidence of an ultrafast two-time scale process at low temperatures, involving exciton-polaron formation within tens of femtoseconds, followed by torsional relaxation on a  $\sim 300$  femtosecond time scale. The second step is the driving force for exciton migration, as initial conjugation breaks are removed by dynamical planarization. The quantum coherent nature of the elementary exciton migration step is consistent with experimental observations highlighting the correlated and vibrationally coherent nature of the dynamics on ultrafast time scales.

The photogeneration and spatial migration of excitons is of key importance in organic electronic materials [1]. Molecular excitons in these  $\pi$ -conjugated organic semiconductors are bound electron-hole pairs delocalized over one to ten monomer units [2–4], whose diffusion length typically falls into a 10 nm range. The basic entities subject to photoexcitation have also been termed chromophores, or spectroscopic units [3, 5], and have been identified with conformational subunits delimited by conjugation breaks or chemical defects. However, the precise definition of spectroscopic units and their dynamical evolution, at a molecular level, has remained elusive [5, 6].

While conventional ensemble measurements have been limited by conformational averaging, recent single-molecule low-temperature spectroscopy [2] as well as transient electronic spectroscopies [7] and time-resolved Raman studies [8] pave the way for a more detailed understanding of the primary excitations and their dynamics, on time scales ranging from femtoseconds to hundreds of picoseconds. Various studies point to the dominant role of conformational defects along polymer chains, and emphasize that fluctuations from disordered to ordered conformations are favored on short time scales. Torsional relaxation has been conjectured to interfere with excitation energy transfer [9], and the large Stokes shift is indicative of strong exciton-phonon coupling leading to highly correlated motions in a subpicosecond regime [10]. Vibrational quantum coherence was found to persist on time scales of several hundred femtoseconds [11]. Meanwhile, the role of exciton trapping, exciton-polaron formation, and the response of excitonic species to structural changes remain controversial [8, 12].

Theoretical analysis of exciton transport in single chains (i.e., quasi-1D systems) generally relies on a Frenkel-Holstein Hamiltonian [13] description for  $J$ -aggregates, i.e., head-to-tail aligned molecular aggregates [14]. Besides Förster rate theory [1], quantum-classical studies of Ehrenfest type [15] and Surface-Hopping type

[16] have been conducted, all of which are restricted in the treatment of exciton-phonon correlations and may not correctly describe the intricate interplay of electronic delocalization, trapping, and exciton migration. Full quantum dynamical studies have been limited to short oligomer segments where the earliest time scales were found to be dominated by coherent electronic effects [17].

Against this background, the present study employs a high-dimensional quantum dynamical description, using efficient multiconfigurational approaches [18, 19], to elucidate the elementary step of intra-chain exciton migration in the presence of torsional dynamics. We employ an *ab initio* parametrized, generalized  $J$ -aggregate Hamiltonian for an oligothiophene eicosamer (OT-20) representative of a chromophore segment of poly(3-hexylthiophene) (P3HT) which plays a central role as an electron donor

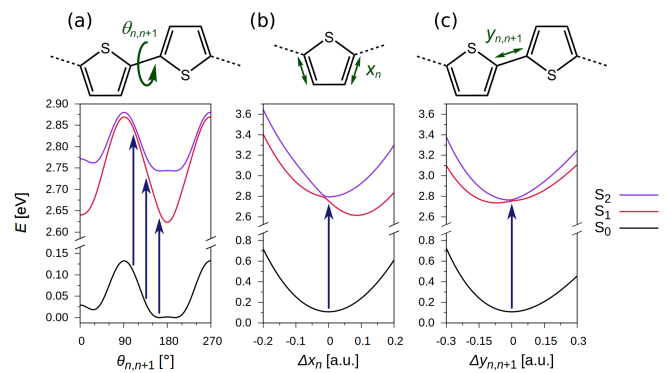


FIG. 1. *Ab initio* based PES sections for an OT-20 oligomer as a function of selected torsional ( $\theta_{n,n+1}$ ), ring-breathing ( $x_n$ ), and inter-monomer bond stretch ( $y_{n,n+1}$ ) coordinates. The electronic ground state ( $S_0$ ) and first two excited singlet states ( $S_1$ ,  $S_2$ ) are shown. Note that the torsional  $S_1$  potential is very stiff as compared with the ground state; also, the local ring-breathing mode exhibits the largest PES shift, giving rise to pronounced exciton trapping effects.

species in organic photovoltaics. The Hamiltonian was constructed by a mapping procedure [20] which transforms oligomer potential energy surfaces (PES) to a site-based Frenkel-Holstein type Hamiltonian. Selected high-level electronic structure calculations were carried out to construct PES sections for several modes exhibiting the most pronounced vibronic coupling effects, i.e., inter-monomer torsional modes ( $\theta_{n,n+1}$ ), symmetric ring-breathing modes ( $x_n$ ), and inter-monomer C-C bond stretch modes ( $y_{n,n+1}$ ), as illustrated in Fig. 1.

The resulting Hamiltonian in the basis of Frenkel configurations  $|n\rangle$ , i.e., single-monomer excitations in the direct-product space spanned by  $N$  monomers, reads

$$\hat{H} = \sum_{n,n'=1}^N \hat{H}_{n,n'} |n\rangle \langle n'| + \hat{H}_{\text{bath}} \hat{1} \quad (1)$$

combining contributions for an  $N$ -site system ( $\hat{H}_{n,n'}$ ) with an external bath ( $\hat{H}_{\text{bath}}$ ). Here,  $\hat{H}_{n,n'}$  comprises kinetic energy ( $\hat{T}$ ) and on-site ( $\hat{V}_n^{\text{site}}$ ) contributions, as well as excitonic couplings ( $\hat{V}_{n,n'}^{\text{exc}}$ ),

$$\hat{H}_{n,n'} = \delta_{n,n'} \hat{T} + \delta_{n,n'} \hat{V}_n^{\text{site}} + \hat{V}_{n,n'}^{\text{exc}} \quad (2)$$

where  $\hat{T}$  corresponds to the kinetic energy operator in curvilinear coordinates [21, 22],

$$\begin{aligned} \hat{T} = \frac{1}{2} & \left( \sum_{n=1}^N G_{xx} \hat{p}_{x_n}^2 + \sum_{n=1}^{N-1} (G_{yy} \hat{p}_{y_{n,n+1}}^2 + G_{\theta\theta} \hat{p}_{\theta_{n,n+1}}^2) \right. \\ & \left. + 2 \sum_{n=1}^N G_{xy} \hat{p}_{x_n} (\hat{p}_{y_{n,n+1}} + \hat{p}_{y_{n,n-1}}) \right) \end{aligned} \quad (3)$$

with  $G_{\theta\theta} = I_{\theta}^{-1}$ ,  $G_{yy} = m_y^{-1}$ , and  $G_{xx} = m_x^{-1}$ . The site potential of Eq. (2) reads as follows,

$$\hat{V}_n^{\text{site}}(\{\hat{x}, \hat{y}, \hat{\theta}\}) = \hat{V}_0(\{\hat{x}, \hat{y}, \hat{\theta}\}) + \hat{\Delta}_n(\hat{x}_n, \hat{y}_{n,n\pm 1}, \hat{\theta}_{n,n\pm 1}) \quad (4)$$

with the ground-state potential

$$\hat{V}_0(\{\hat{x}, \hat{y}, \hat{\theta}\}) = \sum_{l=1}^N \hat{v}_G(\hat{x}_l, \hat{y}_{l,l\pm 1}, \hat{\theta}_{l,l\pm 1}) \quad (5)$$

and the difference potential

$$\begin{aligned} \hat{\Delta}_n(\hat{x}_n, \hat{y}_{n,n\pm 1}, \hat{\theta}_{n,n\pm 1}) = & c_E + \hat{v}_E(\hat{x}_n, \hat{y}_{n,n\pm 1}, \hat{\theta}_{n,n\pm 1}) \\ & - \hat{v}_G(\hat{x}_n, \hat{y}_{n,n\pm 1}, \hat{\theta}_{n,n\pm 1}) \end{aligned} \quad (6)$$

where  $c_E$  is a constant excitation energy and  $\hat{v}_G$  and  $\hat{v}_E$  are ground-state and excited-state monomer potentials. Further, the excitonic couplings of Eq. (2) are given as

$$\hat{V}_{n,n\pm 1}^{\text{exc}}(\hat{\theta}_{n,n\pm 1}) = \hat{w}(\hat{\theta}_{n,n\pm 1}) \quad (7)$$

where an additional dependence on the high-frequency modes  $\hat{x}_n$  and  $\hat{y}_{n,n\pm 1}$  has been neglected. The functions

$v_G$  and  $v_E$  (including edge effects [22]), along with  $w$  and the constant  $c_E$  are determined by the solution of an inverse eigenvalue problem as described in Ref. [20]. In the present case, the functional forms correspond to Morse potentials and a cosine series, respectively [20, 22].

Finally, the bath Hamiltonian of Eq. (1) corresponds to a collection of harmonic oscillators coupled to the torsional modes  $\theta$ ,

$$\hat{H}_{\text{bath}}(\{\hat{b}\}) = \sum_j \frac{\hat{p}_{b,j}^2}{2} + \frac{\omega_j^2}{2} (\hat{b}_j - \frac{c_j}{\omega_j^2} (\hat{\theta}_{n,n+1} - \theta_0))^2 \quad (8)$$

where the couplings  $c_j$  are adapted to an Ohmic spectral density,  $c_j = \omega_j \sqrt{(2/\pi)\gamma I_{\theta} \Delta\omega}$  with  $\gamma$  the friction coefficient

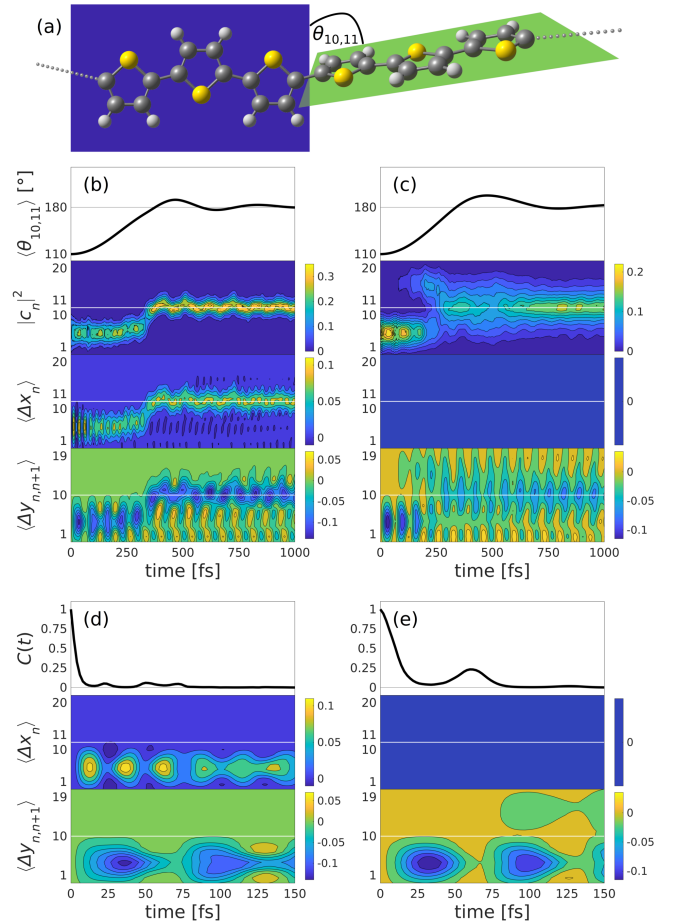


FIG. 2. (a) Schematic illustration of the OT oligomer system under investigation, (b) for a simulation set-up including all modes, expectation value of the central torsion ( $\langle \theta \rangle_{10,11}$ ), squared coefficients of the excitonic wavefunction ( $|c_n|^2$ ), expectation values of the high-frequency modes relative to their equilibrium position ( $\langle \Delta x_n \rangle = \langle \hat{x}_n \rangle - \langle \hat{x}_n \rangle_0$ ) and analogously for  $\langle \Delta y_{n,n+1} \rangle$ ), (c) analogous results for a simulation set-up excluding the local modes  $\{x_n\}$ , (d) on a shorter time scale (150 fs), the decay of the transition dipole autocorrelation function  $C(t)$  is shown, along with expectation values of the high-frequency modes, (e) analogously,  $C(t)$  in the absence of the local modes  $\{x_n\}$ .

cient and  $\Delta\omega$  the frequency spacing that determines the Poincaré recurrence time  $T_P = 2\pi/\Delta\omega$ .

Quantum dynamical simulations were performed using the Multi-Layer Multiconfiguration Time-Dependent Hartree (ML-MCTDH) method [18, 19] (Heidelberg MCTDH package [23]), comprising eight layers encompassing 50 phonon degrees of freedom and 20 electronic states [22]. To reduce the computational effort, we only include the central inter-monomer torsion of the OT-20 segment, i.e.,  $\theta_{10,11}$ , with an initial displacement at  $\theta_{10,11} = 110^\circ$ , and keep all other inter-monomer torsions fixed at the ground-state equilibrium geometry,  $\theta_{\text{eq}} = 160^\circ$ . Damping is imposed on  $\theta_{10,11}$  using the harmonic oscillator bath of Eq. (8) comprising a set of at least 10 bath oscillators with a frequency spacing of  $\Delta\omega = 6 \times 10^{-5}$  a.u. and a damping time of  $\gamma^{-1} = 200$  fs.

Prior to real-time calculations, imaginary-time propagation in the electronic subspace was carried out in order to create the initial, partially delocalized exciton state to the left of the torsional defect, which corresponds to the lowest adiabatic eigenstate of the left OT-10 segment.

The exciton evolution up to 1 picosecond, along with the expectation values of the central torsional mode  $\theta_{10,11}$  and the high-frequency modes, as well as the transition dipole autocorrelation function  $C(t) = \text{Tr}\{\hat{\mu}(t)\hat{\mu}|0\rangle\langle 0|\} = \mu_{\text{EG}}^2 \langle \psi(t)\psi(0) \rangle$  [22] are shown in Fig. 2. The excitonic wavefunction is found to remain localized on the left segment during about 300 femtoseconds and is then displaced toward the center of the lattice, as the central torsion planarizes. More detailed analysis shows that the interaction of the exciton with the high-frequency vs. low-frequency modes gives rise to two characteristic time scales, as now discussed.

Within the first  $\sim 50$  femtoseconds, the exciton contracts by three monomer units [22], while the intra-

monomer CC bonds ( $x_n$ ) of the left fragment are found to expand and the inter-monomer CC bonds ( $y_{n,n\pm 1}$ ) contract. The concomitant decay of the transition dipole autocorrelation function  $C(t)$  within  $\sim 10$  fs (Fig. 2d) can be related to the experimentally observed polarization anisotropy decay [24]. During the whole simulation, the mode displacements appear to move adiabatically with the exciton – i.e., the exciton is “dressed” by the lattice distortion, forming an exciton-polaron quasi-particle.

Between 300 fs and 400 fs, the exciton-polaron is completely transferred to the center of the chain (Fig. 2b). The transfer is rather sudden and coincides with the dynamical planarization of the active torsional mode  $\theta_{10,11}$ , in excellent agreement with the experimentally observed torsional relaxation time scale of 400 fs [25]. The exciton is now trapped at the center of the chain, while the intra and inter-monomer CC bonds of the left segment return to their ground state equilibrium values. In the absence of the high-frequency local CC modes (Fig. 2c), the trapping effect turns out to be conspicuously less pronounced, and the exciton density appears less compact.

The role of the torsional degree of freedom is best appreciated by analyzing the dependence of the electronic structure on the central torsion  $\theta_{10,11}$ , see Fig. 3. Here, a transition density analysis (TDA) [26, 27] is shown for OT-20, yielding an electron-hole representation  $|n_e n_h\rangle$ , based upon Time-Dependent Density Functional Theory (TDDFT) calculations [22]. The diagonal dominance of the TDA map indicates that the Frenkel model employed in the present study, which is restricted to the center-of-mass exciton ( $n_e = n_h$ ), is a good approximation. As can be inferred from the TDA, the lowest excited electronic state ( $S_1$ ) corresponds to the nodeless Frenkel ground state, or local exciton ground state (LEGS) [12, 15] at  $\theta = 0^\circ$ , while the second excited state ( $S_2$ ) exhibits a central node, in line with the ascending solutions of a  $J$ -type Frenkel model [14, 20]. At  $\theta = 90^\circ$ , though,  $S_1$  exhibits a conjugation break, such that the  $S_1$  and  $S_2$  densities

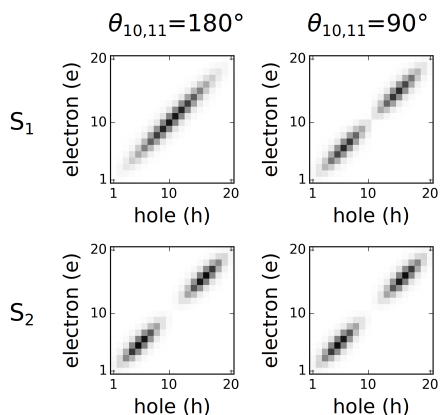


FIG. 3. Electron-hole map, showing occupation probabilities of  $|n_e n_h\rangle$  states, obtained by TDA for OT-20, based on TDDFT calculations. The TDA analysis is shown for the two lowest adiabatic states ( $S_1$ ,  $S_2$ ), for the planar geometry ( $\theta_{10,11} = 180^\circ$ ) and the twisted geometry ( $\theta_{10,11} = 90^\circ$ ).

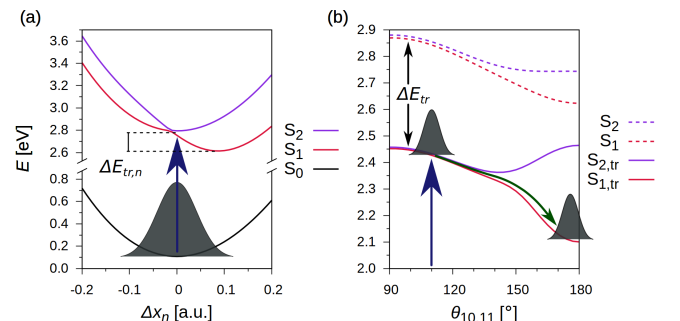


FIG. 4. Main steps of the photoinduced process on coupled ( $S_1, S_2$ ) potentials: (a) Excited-state reorganization of local high-frequency modes  $\{\hat{x}_n\}$  with reorganization (trapping) energy  $\Delta E_{\text{tr},n}$ , (b) torsional relaxation on effective, dressed potentials ( $S_{1,\text{tr}}, S_{2,\text{tr}}$ ) including polaronic stabilization  $\Delta E_{\text{tr}}$ .

are very similar. The transition between these limiting cases happens between 140°-160° [22]. It is this transition which underlies the dynamics observed in Fig. 2.

Fig. 4 illustrates the key steps of the dynamics in terms of the coupled dynamics of the two lowest adiabatic excitonic states [17, 27]. From this viewpoint, the initial state is a left or right localized coherent superposition,  $|\psi_L\rangle = 1/\sqrt{2}(|\psi_{S_1}\rangle + |\psi_{S_2}\rangle)$  or  $|\psi_R\rangle = 1/\sqrt{2}(|\psi_{S_1}\rangle - |\psi_{S_2}\rangle)$ . The initial, localized state is stabilized by trapping *via* the high-frequency modes (Fig. 4a), with typical stabilization energies around  $\Delta E_{\text{tr}} \sim 0.5$  eV. The trapped state is, however, not fully relaxed, and sustained high-frequency oscillations are observed for hundreds of femtoseconds, in line with experiment [11]. As long as the conjugation break persists, both  $S_1$  and  $S_2$  states exhibit density away from the junction between the left/right segments. The situation changes markedly as the system planarizes, such that the  $S_1$  state turns into the nodeless LEGS on the full lattice. During the downhill dynamics on effective, dressed torsional PESs (Fig. 4b), excess energy is absorbed by the external bath modes. This picture is in line with experimental observations indicating correlated exciton relaxation driven by torsional motion [10].

Our analysis supports the notion of spectroscopic units [3, 5], in the sense of conformational subunits whose location and spatial extension dynamically evolves as a function of conformational fluctuations. The present simulations, at  $T = 0K$ , provide a snapshot of such a torsional fluctuation event guiding coherent exciton migration. At higher temperatures, thermally induced torsional fluctuations will lead to multiple exciton migration pathways evolving under the influence of disorder. The high-frequency modes, by contrast, remain unaffected by temperature, preserving the polaronic character of the dressed exciton. The resulting picture corresponds to a Holstein polaron driven by fluctuations.

The present analysis underscores the quasi-particle nature of the exciton and the key role of exciton trapping, in contrast to current interpretation, e.g., in Ref. [12]. However, our results also suggest that the observed dynamics falls into a non-universal parameter regime where exciton binding energies can differ markedly depending on exciton-phonon coupling strength.

By capturing the elusive exciton migration event, the present analysis offers a consistent interpretation of various experimental findings, including the observation of ultrafast polarization anisotropy decay [24], the correlated ultrafast dynamics and large Stokes shift in conjugated polymers featuring torsional modes [10], the interleaved nature of torsional relaxation and excitation energy transfer [9], and the persistence of coherent high-frequency motions in photoexcited conjugated polymers [11]. Thermal effects and the important role of aggregation and aggregation-induced planarization in P3HT [2] can be included in the present model and will be addressed in forthcoming work.

This work was supported by the Deutsche Forschungsgemeinschaft (DFG grant BU-1032-2).

- 
- \* Author to whom correspondence should be addressed: burghardt@chemie.uni-frankfurt.de
- [1] A. Köhler and H. Bässler, *Electronic Processes in Organic Semiconductors* (Wiley-VCH Verlag, Weinheim, Germany, 2015).
  - [2] D. Raitzel, S. Baderschneider, T. B. de Queiroz, R. Lohwasser, J. Köhler, M. Thelakkat, S. Kümmel, and R. Hildner, *Macromolecules* **49**, 9553 (2016).
  - [3] M. M. Grage, P. W. Wood, A. Ruseckas, T. Pullerits, W. Mitchell, P. L. Burn, I. Samuel, and V. Sundström, *J. Chem. Phys.* **118**, 7644 (2003).
  - [4] S. Tretiak, A. Saxena, R. L. Martin, and A. R. Bishop, *Phys. Rev. Lett.* **89**, 097402 (2002).
  - [5] W. Beenken and T. Pullerits, *J. Phys. Chem. B* **108**, 6164 (2004).
  - [6] W. Beenken, *Phys. Status Solidi A* **206**, 2750 (2009).
  - [7] E. Collini and G. D. Scholes, *Science* **323**, 369 (2009).
  - [8] A. E. Bragg, W. Yu, J. Zhou, and T. Magnanelli, *J. Phys. Chem. Lett.* **7**, 3990 (2016).
  - [9] S. Westenhoff, W. Beenken, R. H. Friend, N. C. Greenham, A. Yartsev, and V. Sundström, *Phys. Rev. Lett.* **97**, 166804 (2006).
  - [10] N. P. Wells and D. A. Blank, *Phys. Rev. Lett.* **100**, 086403 (2008).
  - [11] Y. Song, C. Hellmann, N. Stingelin, and G. D. Scholes, *J. Chem. Phys.* **142**, 212410 (2015).
  - [12] W. Barford and M. Marcus, *J. Chem. Phys.* **146**, 130902 (2017).
  - [13] T. Holstein, *Ann. Phys. (N. Y.)* **8**, 325 (1959).
  - [14] F. C. Spano and C. Silva, *Ann. Rev. Phys. Chem.* **65**, 477 (2014).
  - [15] O. R. Tozer and W. Barford, *J. Phys. Chem. A* **116**, 10310 (2012).
  - [16] T. Nelson, S. Fernandez-Alberti, A. E. Roitberg, and S. Tretiak, *J. Phys. Chem. Lett.* **8**, 3020 (2017).
  - [17] R. Binder, J. Wahl, S. Römer, and I. Burghardt, *Faraday Discuss.* **163**, 205 (2013).
  - [18] M. H. Beck, A. Jäckle, G. A. Worth, and H. D. Meyer, *Phys. Rep.* **324**, 1 (2000).
  - [19] H. Wang, *J. Phys. Chem. A* **119**, 7951 (2015).
  - [20] R. Binder, S. Römer, J. Wahl, and I. Burghardt, *J. Chem. Phys.* **141**, 014101 (2014).
  - [21] D. Lauvergnat and A. Nauts, *J. Chem. Phys.* **116**, 8560 (2002).
  - [22] See Supplemental Material at [ ] for simulation details.
  - [23] G. A. Worth, M. H. Beck, A. Jäckle, and H. Meyer, "The MCTDH package," (2015), see <http://www.pci.uni-heidelberg.de/tc/usr/mctdh/>.
  - [24] M. M. Grage, Y. Zaushitsyn, A. Yartsev, M. Chachisvilis, V. Sundström, and T. Pullerits, *Phys. Rev. B* **67**, 205207 (2003).
  - [25] J. Zhou, W. Yu, and A. E. Bragg, *J. Phys. Chem. Lett.* **6**, 3496 (2015).
  - [26] S. Tretiak and S. Mukamel, *Chem. Rev.* **102**, 3171 (2002).
  - [27] A. N. Panda, F. Plasser, A. Aquino, I. Burghardt, and H. Lischka, *J. Phys. Chem. A* **117**, 2181 (2013).